Suppl. ^{234}Th based global estimates of particulate and dissolved organic carbon downward export fluxes in the ocean

Wei-Lei Wang[1], Frédéric A. C. Le Moigne[2,3], François W. Primeau[1], J. Keith Moore[1]

[1]Department of Earth System Science, University of California at Irvine, Irvine, CA 92697, USA.

[2]GEOMAR, Helmholtz Centre for Ocean Research Kiel, Kiel, Germany.

[3]Mediterranean Institute of Oceanography (MIO), UM110, CNRS, IRD, Aix-Marseille Université, Campus de Luminy, 13288, Marseille, France

1 Supplementary Methods

1.1 Data

Total ^{234}Th (particulate+dissolved) activity are obtained by compiling data from GEOTRACES [*Mawji et al.*, 2015; *Schlitzer et al.*, 2018] and from published reference (Table S1). Globally, we have a total of 3723 measurements from the literature and 2262 from US GEOTRACES. After binning these observations into the grid of the Ocean Circulation Inverse Model (OCIM) (2°× 2° resolution with 24 vertical levels), there are 2521 grid boxes with ^{234}Th measurements (Fig. 1). ^{234}Th based upper ocean (<150 m) POC flux data are from https://www.pangaea.de/ [*Le Moigne et al.*, 2013], with new data from *Black et al.* [2018]. The inverse model also uses salinity, phosphate, and net primary production (NPP) data. The salinity and inorganic phosphorus data are from World Ocean Atlas 2013 [*Zweng et al.*, 2013; *Garcia et al.*, 2014]. Net primary production (NPP) data used to parameterize biological phosphate uptake are satellite-derived carbon based primary production data (MODIS CbPM) [*Westberry et al.*, 2008]. Sediment POC flux data are downloaded from https://doi.pangaea.de/10.1594/PANGAEA.855600 [*Mouw et al.*, 2016], and are binned into the grid of OCIM.

Corresponding author: W. L. Wang, weilei.wang@gmail.com

1.2 Circulation and particle sinking models

Dissolved ^{234}Th and phosphate are transported by advection and diffusion that are modeled using an advection-diffusion transport operator, $\mathbf{T}$, defined so that $\mathbf{T}[C] \equiv \nabla \cdot \left(\vec{U}[C] - \mathbf{K}\nabla[C]\right)$. This operator was optimized using multiple tracers, including salinity, temperature, sea surface height, CFC11, pre-bomb radiocarbon, and phosphate [*DeVries and Primeau*, 2011; *Primeau et al.*, 2013]. Element concentrations are denoted using square bracket (e.g. [C]). The vertical transport of particulate ^{234}Th and particulate organic phosphorus is modeled using a particle flux divergence operator that is built based on the power law attenuation function known as Martin curve [*Fu and Primeau*, 2017]. The Martin curve exponential b values are optimized in inversion,

1.3 Bayesian optimization

We obtain P and Th fields by solving the governing equations for P and Th(Eqs.1-3). The governing equations for P-cycle model are linear, and thus can be solved using direct matrix inversion. With POP concentration from the P model, the Th equations are also linear, and are therefore solved by direct matrix inversion. We minimize the difference between model outputs and observations by optimizing a set of parameters controlling P and Th cycle using the following objective function.

$$f = {e_{\mathrm{P}}}' \frac{1}{\mathbf{W_P}} e_{\mathrm{P}} + {e_{\mathrm{Th}}}' \frac{1}{\mathbf{W_{Th}}} e_{\mathrm{Th}},$$

where $e_{\mathrm{Th}} = \log(\mathrm{Th}_{\mathrm{mod}}) - \log(\mathrm{Th}_{\mathrm{obs}})$ and $e_{\mathrm{P}} = \log(\mathrm{DIP}_{\mathrm{mod}}) - \log(\mathrm{DIP}_{\mathrm{obs}})$. $\mathbf{W_{Th}}$ and $\mathbf{W_P}$ are weighing matrices for ^{234}Th and DIP. $\mathbf{W_{Th}}$ is defined using the following equation,

$$\mathbf{W_{Th}} = \frac{1}{\sigma^2_{\mathrm{Th}}} \mathbf{V},$$

where $\mathbf{V}$ is grid-box fractional volumes, and σ_{Th} is defined,

$$\sigma^2_{\mathrm{Th}} = (\log(\mathrm{Th}_{\mathrm{mod}}) - \mu_{\mathrm{Th}})' \mathbf{V} (\log(\mathrm{Th}_{\mathrm{mod}}) - \mu_{\mathrm{Th}})$$

with

$$\mu_{\mathrm{Th}} = \frac{\Sigma(\log(\mathrm{Th}_{\mathrm{obs}})\mathbf{V_{Th}})}{\Sigma \mathbf{V_{Th}}},$$

where $\mathbf{V_{Th}}$ is grid box volume, and the subscript Th represents the grid boxes with ^{234}Th observations. The DIP weighing matrix $\mathbf{W_P}$ is defined similarly.

The optimization is conducted using a matlab function fminunc, which is efficient because we are able to supply the first and second derivatives. The optimization are generally finish within 100 iterations. The optimal model parameters are presented in Table S2 and Fig. S1. Parameter errorbars that correspond to ± 1 standard deviation, are calculated according to *Wang et al.* [2019]

1.4 Error estimation

The error estimation is conducted using Monte Carlo method. Errors are considered from three major sources. 1) model parameters and associated error bars, 2) C:P ratio that is used to convert total phosphorus export to carbon export, 3) POC to ^{234}Th ratio. For each iteration, parameters are randomly drawn from a normal distribution with mean defined by optimal model parameters and variance defined by the covariance matrix (second derivative Hessian matrix evaluated at optimal parameter values). C:P ratio from Teng et al is randomly selected from a space that constrained by the errorbar ranges for each region. POC to ^{234}Th ratio is drawn from a normal distribution with a mean defined by POC:Th $= 135.3z^{-0.795}$ at $z = 114$m and a variance of 0.25, which creates a range between $\sim$2.3 to $\sim$4.0 that is consistent to Fig. 8 of Ref.[*Owens et al.*, 2015]. In the Monte Carlo analysis, we recalculate carbon export fluxes based on parameters from each random drawn. The median values and 95% confidence intervals are based on a sample size of 1000.

1.5 Sensitivity tests

In the model, we use particulate organic phosphorus [POP] as a proxy for sinking particles that carries ^{234}Th out of the surface ocean. We acknowledge that phosphorus is a small portion of sinking particles, other components, such as particulate organic carbon, opal, and calcium carbonate, also absorb dissolved thorium. Here we run multiple sensitivity tests to demonstrate that our model is robust to $R_{M:P}$, sinking mass to phosphorus ratio.

In the first test, we converted POP to POC by applying spatially variable C:P ratios based on *Galbraith and Martiny* [2015]. We tested if the converted [POC] is a better proxy for the sinking particles because carbon is a larger portion of sinking particles compared to phosphorus. However, we reject this model based on its poor model ver-

sus observation fittings (Fig. S3). One possible reason for the poor performance is that POC may not represent sinking mass better than phosphorus. One can image that in high productivity regions, such as the Southern Ocean, C:P ratio is low according to *Galbraith and Martiny* [2015], but total sinking mass (summation of organic matter, calcium carbonate and opal etc.) to P ratio can be high due to high diatom activities.

In a second experiment, we formulate two equations for sinking mass to phosphorus ratio ($R_{M:P}$), in which sinking mass is proportional to ambient phosphorus concentration. Two parameters controlling the "slope" (S) and "intercept" (R_{min}) are optimized in the inversion (Eq. 3).

$$\begin{aligned} R_{M:P} &= R_{min} + S(1 - tanh([DIP])) \\ R_{M:P} &= R_{min} - S[DIP] \end{aligned} \tag{1}$$

We found that the optimal value of R_{min} correlates with adsorption and desorption rate constants, and the optimal value of S is less than 1×10^{-2}. Thus, we got virtually the same POC and DOC export patterns as the control model. Based on the current data constraints, we did not find the evidence indicating $R_{M:P}$ has spatial variations, and the gradient is too weak and can be ignored.

2 C:P ratio of sinking particles

With the optimal b values and an assumed particle dissolution rate constant, one can estimate particle sinking velocity[*Kriest and Oschlies*, 2008], with which POP sinking flux can be calculated given the POP distribution from the P cycle model. We have POC sinking flux diagnosed from ^{234}Th flux and POC/^{234}Th ratio. We then compute C:P ratio of sinking particles for each region reported in *Teng et al.* [2014]. The results are summarized in Table 3. C:P ratios in the current study are highly correlated to those of *Teng et al.* [2014], and follow the general pattern that C:P ratio is high in the subtropical gyres and low in the high nutrient upwelling regions.

Table 1. Sampling year, area, number of samples (N), how thorium was measured (Methods), and reference of ^{234}Th data.

Year	Regions	*N*	Methods	Reference
1992	Southern Ocean	124	Part.+Diss.	*Van Der Loeff et al.* [1997]
1996	Subarctic Pacific	161	Part.+Diss.	*Charette et al.* [1999]
1993-1994	Middle Atlantic Bight	64	Part.+Diss.	*Santschi et al.* [1999]
1999	Southern Ocean	50	Part.+Diss.	*Coppola et al.* [2005]
2002	Southern Ocean	120	Total	*Buesseler et al.* [2005]
2004	Atlantic (50S-50N)	88	Total	*Thomalla et al.* [2006]
2003-2005	Arctic	38	Total	*Lalande et al.* [2008]
2004	South China Sea	174	Total	*Cai et al.* [2008]
2004-2005	North Atlantic	678	Total	*Buesseler et al.* [2008]
2005	North Pacific	31	Total	*KawaKami et al.* [2010]
2007	Arctic	236	Total	*Cai et al.* [2010]
2008	Southern Ocean	197	Total	*Rutgers van der Loeff et al.* [2011]
2008	South-west Pacific	147	Total	*Zhou et al.* [2012]
2008	Bonus-GoodHope section	175	Total	*Planchon et al.* [2013]
2011	Southern Ocean	185	Total	*Planchon et al.* [2015]
2011	Southern Ocean	318	Total	*Rosengard et al.* [2015]
2012-2013	Southern Ocean	107	Part.+Diss.	*Roca-Martí et al.* [2017]
2009	North Atlantic	97	Total	*Le Moigne et al.* [2013]
2010	North Atlantic	195	Total	*Le Moigne et al.* [2014]
2012	Arctic	98	Total	*Moigne et al.* [2015]
2013	Southern Ocean	127	Total	*Le Moigne et al.* [2016]

Table 2. Most probable parameter values. κ_d is DOP remineralization rate constant. α and β are the two parameters in the function that scales NPP to DIP assimilation rate. κ_1 and κ_{-1} are thorium adsorption and desorption rate constant. Optimal b values are displayed in Fig.1.

Parameters	values	units
κ_d	$(3.78^{+0.06}_{-0.05})\times10^{-8}$	s^{-1}
α	$2.50^{+0.20}_{-0.20}$	s^{-1}
β	$0.71^{+0.01}_{-0.01}$	unitless
κ_1	$(2.69^{+0.04}_{-0.04})\times10^{-5}$	$m^3\ mmol^{-1}s^{-1}$
κ_{-1}	$(9.19^{+0.24}_{-0.24})\times10^{-7}$	s^{-1}

Table 3. Comparison of C:P export ratios between *Teng et al.* [2014] and ^{234}Th based model.

Regions	Teng et al.	This study
N. Atlantic gyre	355^{+65}_{-59}	129^{146}_{106}
Equatorial Atlantic	81^{+21}_{-18}	79^{90}_{65}
S. Atlantic gyre	163^{+49}_{-42}	112^{128}_{93}
Southern Ocean	91^{+11}_{-9}	87^{99}_{72}
S. Indian gyre	115^{+42}_{-35}	125^{143}_{103}
Equatorial Indian Ocean	103^{+30}_{-26}	88^{101}_{73}
S. Pacific gyre	138^{+37}_{-33}	111^{127}_{92}
Equatorial Pacific	83^{+15}_{-13}	80^{91}_{66}
N. Pacific gyre	176^{+33}_{-30}	108^{124}_{90}
N. Subpolar Pacific	86^{+23}_{-20}	74^{85}_{61}
N. subpolar Atlantic	63^{+24}_{-20}	72^{82}_{59}

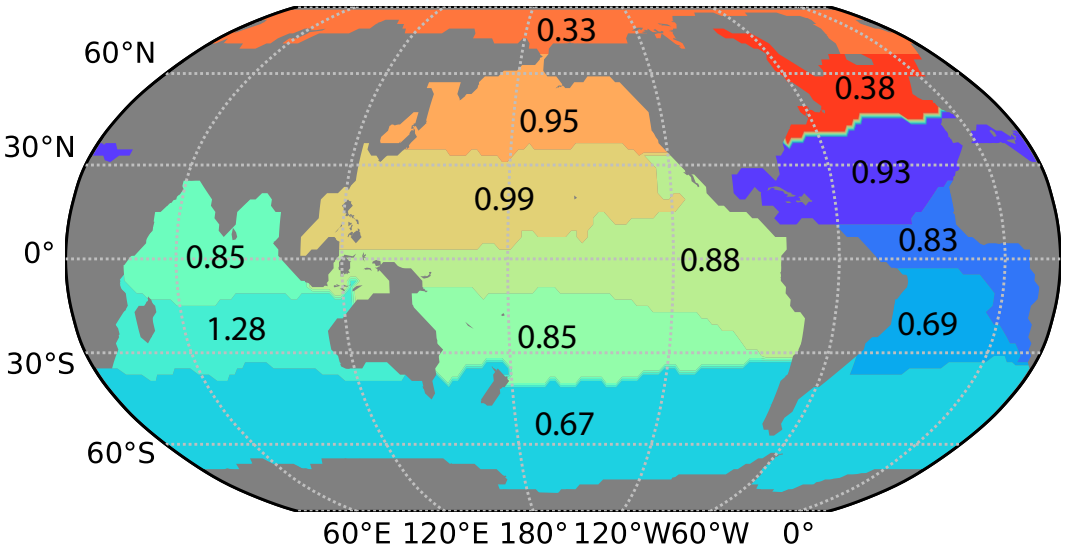

Figure 1. Optimal b values for each region based on *Teng et al.* [2014] division.

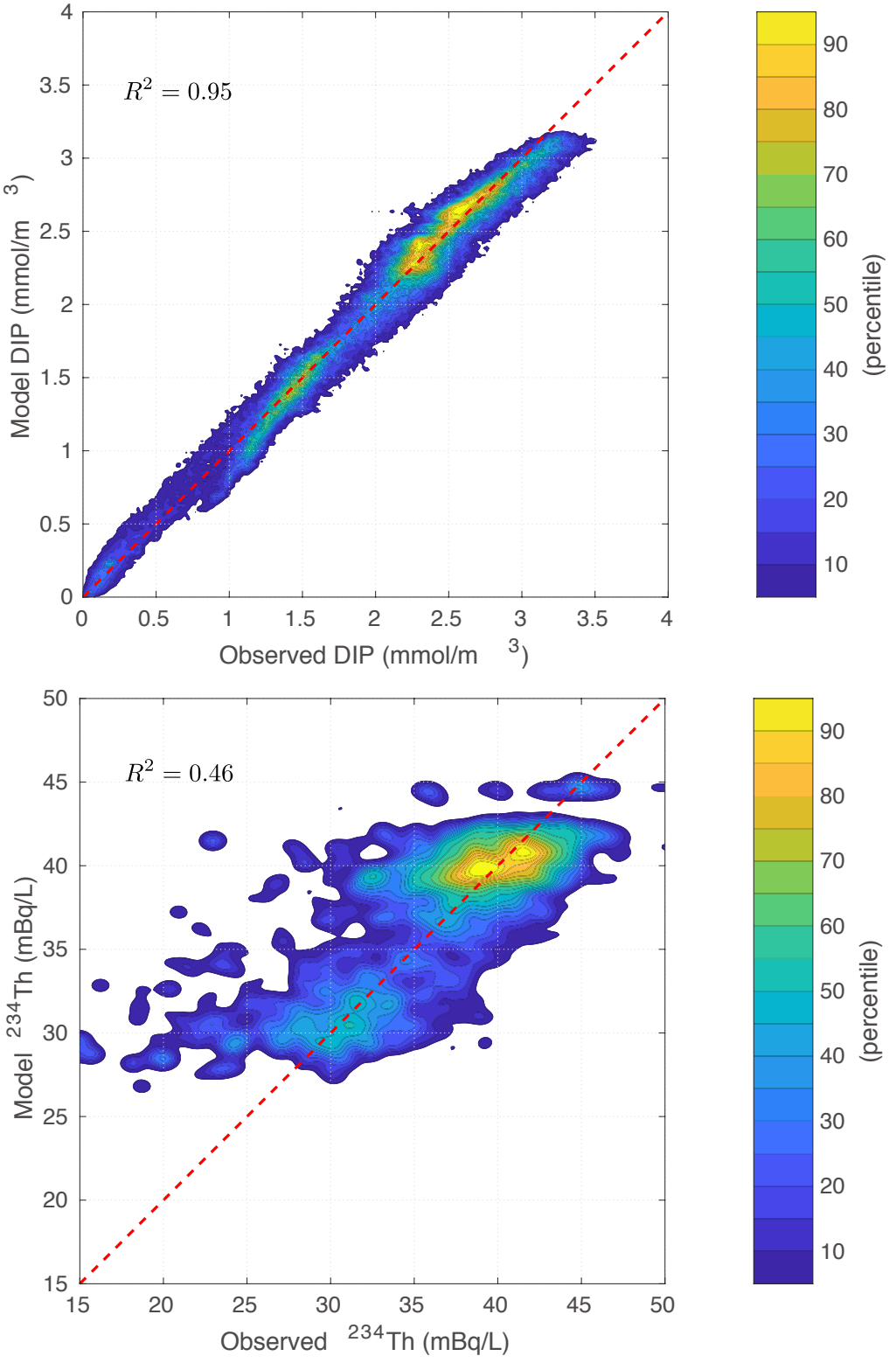

Figure 2. Comparison of model tracers with observed ones. 1) Model DIP versus WOA2013 climatology DIP concentration. 2) Model total 234Th (dissolved + particulate) versus observation.

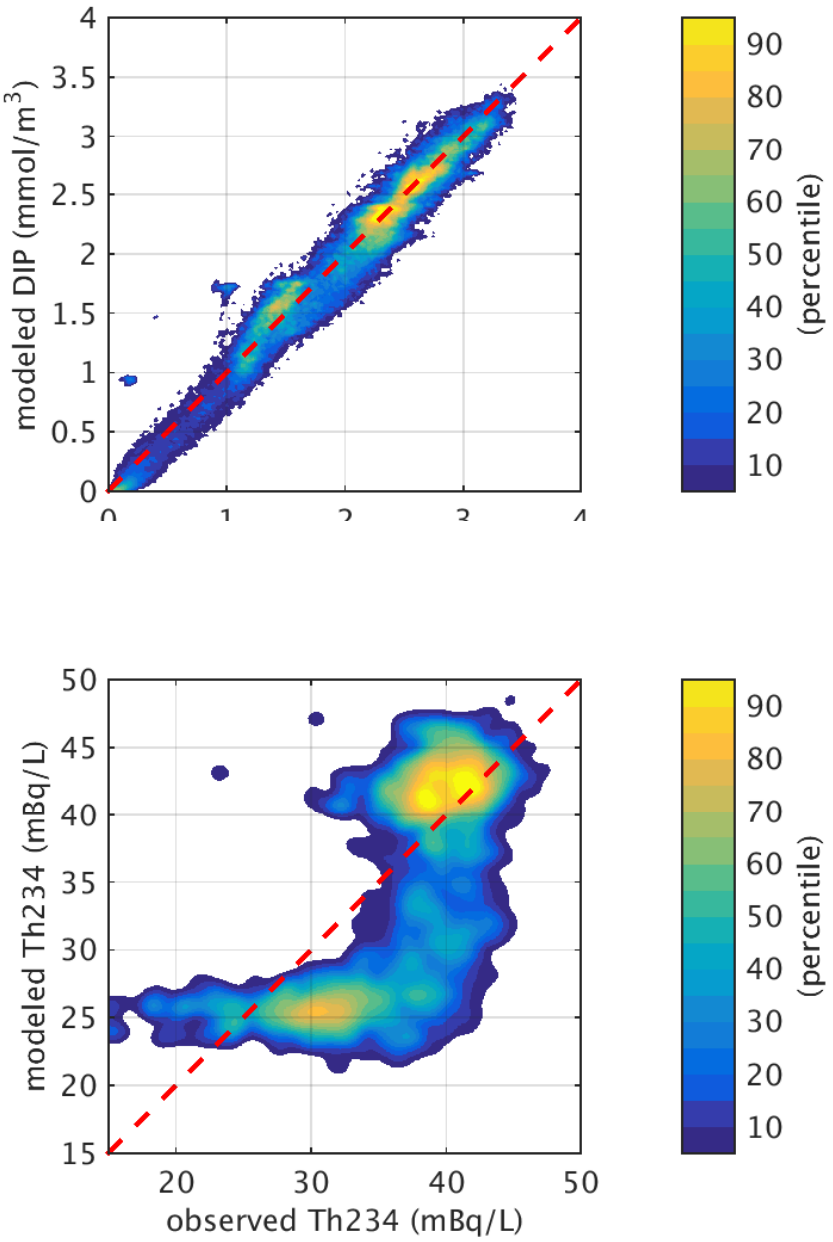

Figure 3. Comparison of observation tracers with model based on Galbraith and Martiny *Galbraith and Martiny* [2015] C:P parameterization. 1) Model DIP versus WOA2013 climatology DIP concentration. 2) Model total 234Th (dissolved + particulate) versus observation.

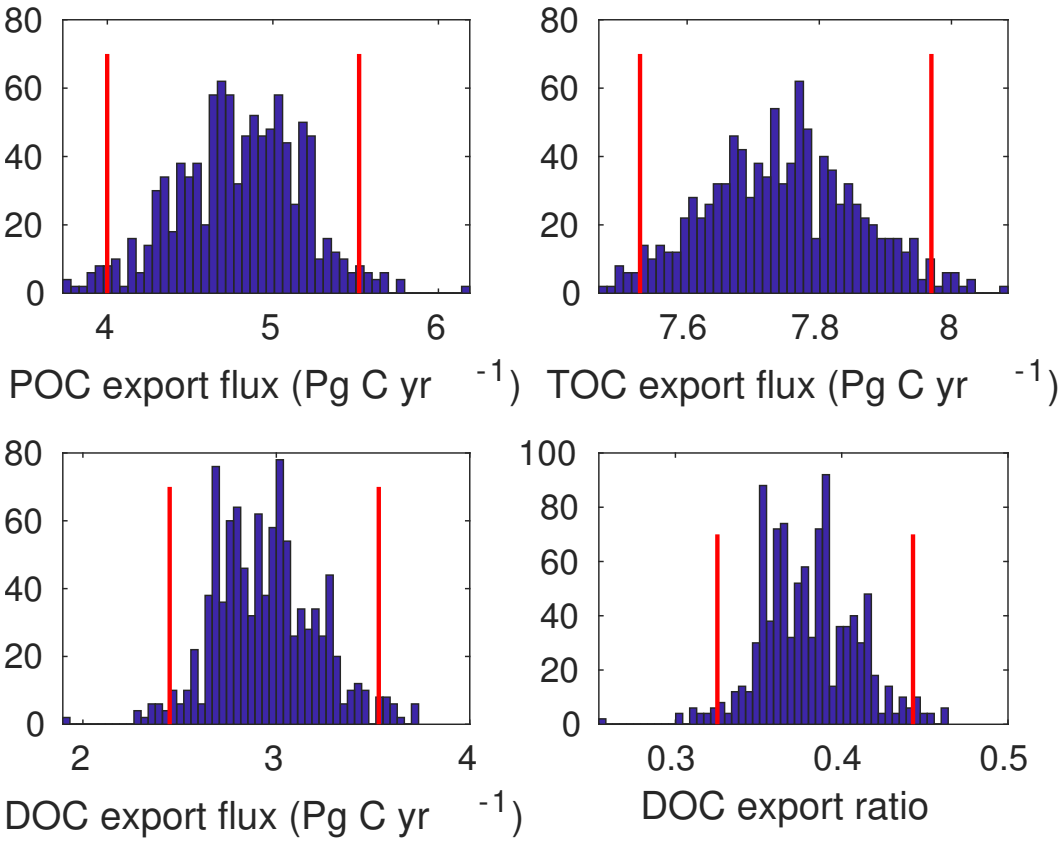

Figure 4. Histogram shows total POC, TOC, and DOC distributions based on Monte Carlo simulation. In the test, we randomly select parameter combinations ($\theta_i \sim N(\hat{\theta}, \Sigma)$), with which we recalculated POC, TOC, and DOC export flux. The model was run 1000 times.

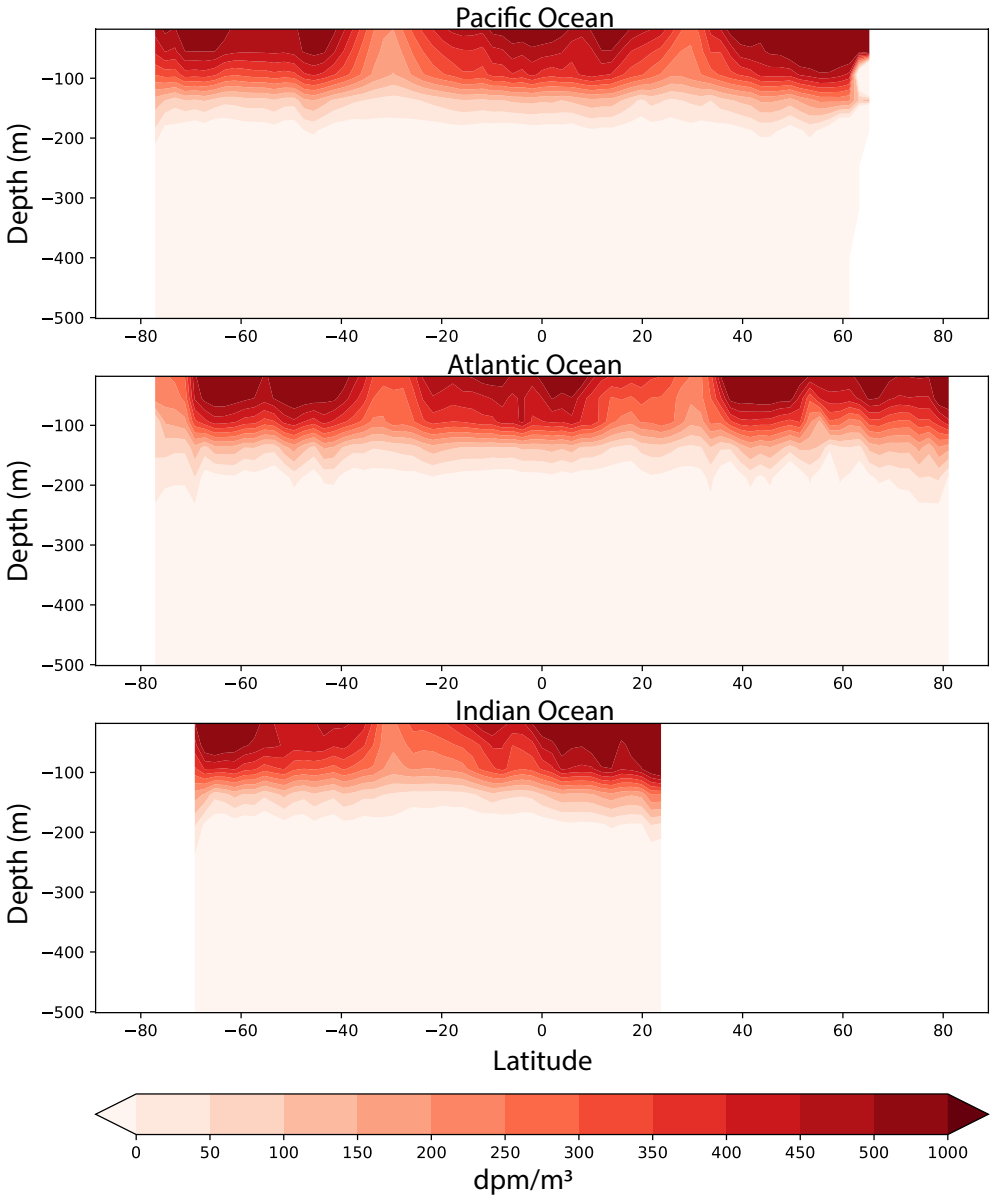

Figure 5. Zonally mean difference between ^{238}U and ^{234}Th for the three major basins.

References

Black, E. E., K. O. Buesseler, S. M. Pike, and P. J. Lam (2018), ^{234}Th as a tracer of particulate export and remineralization in the southeastern tropical Pacific, *Mar. Chem.*, *201*, 35–50, doi:10.1016/j.marchem.2017.06.009.

Buesseler, K. O., J. Andrews, S. M. Pike, M. A. Charette, L. E. Goldson, M. A. Brzezinski, and V. Lance (2005), Particle export during the southern ocean iron experiment (sofex), *Limnology and Oceanography*, *50*(1), 311–327.

Buesseler, K. O., C. Lamborg, P. Cai, R. Escoube, R. Johnson, S. Pike, P. Masque, D. McGillicuddy, and E. Verdeny (2008), Particle fluxes associated with mesoscale eddies in the Sargasso Sea, *Deep-Sea Res. II*, *55*(10-13), 1426–1444, doi:10.1016/j.dsr2.2008.02.007.

Cai, P., W. Chen, M. Dai, Z. Wan, D. Wang, Q. Li, T. Tang, and D. Lv (2008), A high-resolution study of particle export in the southern south china sea based on 234th: 238u disequilibrium, *Journal of Geophysical Research: Oceans*, *113*(C4).

Cai, P., M. Rutgers Van Der Loeff, I. Stimac, E.-M. Nöthig, K. Lepore, and S. Moran (2010), Low export flux of particulate organic carbon in the central arctic ocean as revealed by 234th: 238u disequilibrium, *Journal of Geophysical Research: Oceans*, *115*(C10).

Charette, M. A., S. B. Moran, and J. K. Bishop (1999), 234th as a tracer of particulate organic carbon export in the subarctic northeast pacific ocean, *Deep Sea Research Part II: Topical Studies in Oceanography*, *46*(11-12), 2833–2861.

Coppola, L., M. Roy-Barman, S. Mulsow, P. Povinec, and C. Jeandel (2005), Low particulate organic carbon export in the frontal zone of the southern ocean (indian sector) revealed by 234th, *Deep Sea Research Part I: Oceanographic Research Papers*, *52*(1), 51–68.

DeVries, T., and F. W. Primeau (2011), Dynamically and observationally constrained estimates of water-mass distributions and ages in the global ocean, *J. Phys. Oceanogr.*, *41*(12), 2381–2401, doi:10.1175/jpo-d-10-05011.1.

Fu, W., and F. Primeau (2017), Application of a fast Newton–Krylov solver for equilibrium simulations of phosphorus and oxygen, *Ocean Model.*, *119*, 35–44.

Galbraith, E. D., and A. C. Martiny (2015), A simple nutrient-dependence mechanism for predicting the stoichiometry of marine ecosystems, *Proc. Natl. Acad. Sci.*

USA, *112*(27), 8199–8204, doi:10.1073/pnas.1423917112.

Garcia, H., R. Locarnini, T. Boyer, J. Antonov, O. Baranova, M. Zweng, J. Reagan, and D. Johnson (2014), World Ocean Atlas 2013, Volume 4: Dissolved Inorganic Nutrients (Phosphate, Nitrate, Silicate), NOAA Atlas NESDIS, vol. 76, edited by S. Levitus, 25 pp, *US Gov. Print. Off., Washington, DC*.

KawaKami, H., M. C. Honda, K. Matsumoto, T. Fujiki, and S. Watanabe (2010), East-west Distribution of POC fluxes estimated from ^{234}Th in the northern North Pacific in Autumn, *Journal of Geophysical*, *66*, 71–83.

Kriest, I., and A. Oschlies (2008), On the treatment of particulate organic matter sinking in large-scale models of marine biogeochemical cycles, *Biogeosciences (BG)*, *5*, 55–72.

Lalande, C., S. B. Moran, P. Wassmann, J. M. Grebmeier, and L. W. Cooper (2008), 234th-derived particulate organic carbon fluxes in the northern barents sea with comparison to drifting sediment trap fluxes, *Journal of Marine Systems*, *73*(1-2), 103–113.

Le Moigne, F. A., C. M. Moore, R. J. Sanders, M. Villa-Alfageme, S. Steigenberger, and E. P. Achterberg (2014), Sequestration efficiency in the iron-limited north atlantic: Implications for iron supply mode to fertilized blooms, *Geophysical Research Letters*, *41*(13), 4619–4627.

Le Moigne, F. A., S. A. Henson, E. Cavan, C. Georges, K. Pabortsava, E. P. Achterberg, E. Ceballos-Romero, M. Zubkov, and R. J. Sanders (2016), What causes the inverse relationship between primary production and export efficiency in the Southern Ocean?, *Geophys. Res. Lett.*, *43*(9), 4457–4466.

Le Moigne, F. A. C., S. A. Henson, R. J. Sanders, and E. Madsen (2013), Global database of surface ocean particulate organic carbon export fluxes diagnosed from the ^{234}Th technique, *Earth Syst. Sci. Data*, *5*(2), 295–304, doi:10.5194/essd-5-295-2013.

Mawji, E., R. Schlitzer, E. M. Dodas, C. Abadie, W. Abouchami, R. F. Anderson, O. Baars, K. Bakker, M. Baskaran, N. R. Bates, et al. (2015), The geotraces intermediate data product 2014.

Moigne, F. A., A. J. Poulton, S. A. Henson, C. J. Daniels, G. M. Fragoso, E. Mitchell, S. Richier, B. C. Russell, H. E. Smith, G. A. Tarling, et al. (2015), Carbon export efficiency and phytoplankton community composition in the at-

lantic sector of the arctic ocean, *Journal of Geophysical Research: Oceans*, *120*(6), 3896–3912.

Mouw, C. B., A. Barnett, G. A. McKinley, L. Gloege, and D. Pilcher (2016), Global ocean particulate organic carbon flux merged with satellite parameters, *Earth Syst. Sci. Data*, *8*(2), 531.

Owens, S. A., S. Pike, and K. O. Buesseler (2015), Thorium-234 as a tracer of particle dynamics and upper ocean export in the Atlantic Ocean, *Deep-Sea Res. II*, *116*, 42–59, doi:10.1016/j.dsr2.2014.11.010.

Planchon, F., A.-J. Cavagna, D. Cardinal, L. A. , and F. Dehairs (2013), Late summer particulate organic carbon export and twilight zone remineralisation in the Atlantic sector of the Southern Ocean, *Biogeosciences*, *10*, 803–820, doi:0.5194/bg-10-803-2013.

Planchon, F., D. Ballas, A. Cavagna, A. Bowie, D. Davies, T. Trull, E. Laurenceau-Cornec, P. Van Der Merwe, and F. Dehairs (2015), Carbon export in the naturally iron-fertilized kerguelen area of the southern ocean based on the 234 th approach, *Biogeosciences*, *12*(12), 3831–3848.

Primeau, F. W., M. Holzer, and T. DeVries (2013), Southern Ocean nutrient trapping and the efficiency of the biological pump, *J. Geophys. Res. Ocean.*, *118*(5), 2547–2564, doi:10.1002/jgrc.20181.

Roca-Martí, M., V. Puigcorbé, M. H. Iversen, M. R. van der Loeff, C. Klaas, W. Cheah, A. Bracher, and P. Masqué (2017), High particulate organic carbon export during the decline of a vast diatom bloom in the atlantic sector of the southern ocean, *Deep Sea Research Part II: Topical Studies in Oceanography*, *138*, 102–115.

Rosengard, S. Z., P. J. Lam, W. M. Balch, M. E. Auro, S. Pike, D. Drapeau, and B. Bowler (2015), Carbon export and transfer to depth across the southern ocean great calcite belt, *Biogeosciences*, *12*(13), 3953–3971.

Rutgers van der Loeff, M., P. H. Cai, I. Stimac, A. Bracher, R. Middag, M. B. Klunder, and S. M. A. C. van Heuven (2011), ^{234}Th in surface waters: Distribution of particle export flux across the Antarctic Circumpolar Current and in the Weddell Sea during the GEOTRACES expedition ZERO and DRAKE, *Deep-Sea Res. II*, *58*(25-26), 2749–2766, doi:10.1016/j.dsr2.2011.02.004.

Santschi, P. H., L. Guo, I. D. Walsh, M. Quigley, and M. Baskaran (1999), Boundary exchange and scavenging of radionuclides in continental margin waters of the middle atlantic bight: implications for organic carbon fluxes, *Continental Shelf Research*, *19*(5), 609–636.

Schlitzer, R., R. F. Anderson, E. M. Dodas, M. Lohan, W. Geibert, A. Tagliabue, A. Bowie, C. Jeandel, M. T. Maldonado, W. M. Landing, et al. (2018), The geotraces intermediate data product 2017, *Chemical Geology*, *493*, 210–223.

Teng, Y. C., F. W. Primeau, J. K. Moore, M. W. Lomas, and A. C. Martiny (2014), Global-scale variations of the ratios of carbon to phosphorus in exported marine organic matter, *Nat. Geosci.*, *7*(12), 895–898, doi:10.1038/ngeo2303.

Thomalla, S., R. Turnewitsch, M. Lucas, and A. Poulton (2006), Particulate organic carbon export from the north and south atlantic gyres: The 234th/238u disequilibrium approach, *Deep Sea Research Part II: Topical Studies in Oceanography*, *53*(14-16), 1629–1648.

Van Der Loeff, M. M. R., J. Friedrich, and U. V. Bathmann (1997), Carbon export during the spring bloom at the antarctic polar front, determined with the natural tracer 234th, *Deep Sea Research Part II: Topical Studies in Oceanography*, *44*(1-2), 457–478.

Wang, W., J. Moore, A. Martiny, and F. Primeau (2019), Convergent estimates of marine nitrogen fixation, *Nature*, *566*(7743), 205–+.

Westberry, T., M. Behrenfeld, D. Siegel, and E. Boss (2008), Carbon-based primary productivity modeling with vertically resolved photoacclimation, *Global Biogeochem. Cycles.*, *22*(2), GB2024.

Zhou, K., S. D. Nodder, M. Dai, and J. Hall (2012), Insignificant enhancement of export flux in the highly productive subtropical front, east of new zealand: a high resolution study of particle export fluxes based on 234 th: 238 u disequilibria, *Biogeosciences*, *9*(3), 973–992.

Zweng, M., J. Reagan, J. Antonov, R. Locarnini, A. Mishonov, T. Boyer, H. Garcia, O. Baranova, D. Johnson, D.Seidov, and M. Biddle (2013), World Ocean Atlas 2013, Volume 2: Salinity, NOAA Atlas NESDIS 74, edited by S. Levitus, 39 pp.